

# Digital Alchemy for Materials Design: Colloids and Beyond

Greg van Anders,<sup>1</sup> Daphne Klotsa,<sup>1,2,3</sup> Andrew S. Karas,<sup>1</sup> Paul M. Dodd,<sup>1</sup> and Sharon C. Glotzer<sup>1,4,5</sup>

<sup>1</sup>*Department of Chemical Engineering, University of Michigan, Ann Arbor, MI 48109-2136, USA*

<sup>2</sup>*School of Engineering and Applied Sciences, Harvard University, Cambridge, Massachusetts 02138, USA*

<sup>3</sup>*Department of Chemistry, University of Cambridge, Lensfield Road, Cambridge CB2 1EW, UK*

<sup>4</sup>*Department of Materials Science and Engineering, University of Michigan, Ann Arbor, MI 48109-2136, USA*

<sup>5</sup>*Biointerfases Institute, University of Michigan, Ann Arbor, MI 48109-2800, USA*

Starting with the early alchemists, a holy grail of science has been to make desired materials by modifying the attributes of basic building blocks. Building blocks that show promise for assembling new complex materials can be synthesized at the nanoscale with attributes that would astonish the ancient alchemists in their versatility. However, this versatility means that making direct connection between building block attributes and bulk behavior is both necessary for rationally engineering materials, and difficult because building block attributes can be altered in many ways. Here we show how to exploit the malleability of the valence of colloidal nanoparticle “elements” to directly and quantitatively link building block attributes to bulk behavior through a statistical thermodynamic framework we term “digital alchemy”. We use this framework to optimize building blocks for a given target structure, and to determine which building block attributes are most important to control for self assembly, through a set of novel thermodynamic response functions, moduli and susceptibilities. We thereby establish direct links between the attributes of colloidal building blocks and the bulk structures they form. Moreover, our results give concrete solutions to the more general conceptual challenge of optimizing emergent behaviors in nature, and can be applied to other types of matter. As examples, we apply digital alchemy to systems of truncated tetrahedra, rhombic dodecahedra, and isotropically interacting spheres that self assemble diamond, FCC, and icosahedral quasicrystal structures,

Mendeleev’s tabular organization of the elements [1, 2] by atomic valence [3] has served for more than 140 years as a heuristic that relates properties of the atomic elements to how they arrange in bulk structures. However, attempts to understand how properties of bulk structures relate to atomic properties predate Mendeleev and, in fact, modern science [4], and are complicated by the fact that the chemical manipulation of atoms is prohibited by the quantization of both electrical charge and angular momentum. Fortunately for Mendeleev, this quantization constrains Nature to only about 80 stable elements, and limits elemental properties and bulk behaviors so that the elements can be tabulated by valence. In fact, starting with technetium [5] in the 1930s, new atomic elements have only been produced artificially (as suggested by the etymology of the name “technetium” [6]) by  $\alpha$ -particle bombardment, fusion, or other nuclear techniques that finally realized the ancient alchemists’ goal of transmuting the elements.

In contrast, an inexhaustible array of new “elements” can be synthesized as patchy particles.[7, 8] However, the exploding diversity of patchy particles [8–10] or, more generally, colloidal “elements” means that there are now so many types to synthesize and study that synthesizing them all and determining their bulk behavior is no longer possible in practice. This fundamental impracticality means that, for colloid science to progress, scientists must first ask and answer the basic but daunting question “What elements should I make?” Materials science that starts with this question must be carried out in a fundamentally different way than traditional approaches, guided by the question: What is the optimal building block to make for a given structure, and why is it optimal?

Constructing a periodic table of colloidal elements is easier said than done, however, because, unlike for atoms, colloid valence [11–15] is not discrete. Moreover, entropic colloid valence [14, 16] is a collective effect [17] that emerges only

when colloids are crowded [14, 16]. A first step in constructing a periodic table of colloidal elements was taken by heuristically classifying building blocks according to their valence along anisotropy dimensions [8, 14] that systematically and orthogonally vary colloidal element attributes. This sort of colloidal alchemy is now possible.

Here we present a statistical thermodynamic framework that forms the basis for a new computational approach to building block design, which we term digital alchemy. Using this framework: (i) We show how to treat anisotropy dimensions [8, 14] or other particle interaction parameters as thermodynamic variables, and interpret their conjugate quantities. Treating particle interaction parameters thermodynamically means that the attributes of the colloidal “elements” we study can change so we refer to our methods as “alchemy” The term alchemy has been used previously in the modern era in the context of materials design, and these uses are either different in spirit from the present work [18], or are focused on computing global free energy differences in systems [19, 20] in which intermediate state points are unphysical. A related investigation was also carried out in Ref. [21], which considered the effects of non-rigid colloid shape on crystallization mechanically, whereas here we study rigid colloids that fluctuate thermally. Though there are many systematic investigations of how particle shape or interactions affect structure [10, 14, 22–43], we are aware of no work that attempts to directly probe the thermodynamic response of a system to a change in the attributes of its constituent building blocks. in analogy with pre-scientific attempts to modify chemical elements.[4] (ii) We show how constitutive relations between anisotropy parameters and the thermodynamically conjugate variables we term “alchemical potentials” encode a broad class of detailed quantitative relations between building block attributes and bulk behavior. Further, we define new moduli and susceptibilities that describe stress-strain rela-

tionships between bulk structure and particle attributes. (iii) We show that these building block vs. bulk relationships persist in systems with entropy-driven, emergent collective behavior. (iv) We show how building block vs. bulk relationships can be used both to determine optimal particle shapes or interactions for given structures, and to compute the relative importance of different particle attributes for bulk behavior. (v) We report a detailed, general microscopic design rule for a macroscopic, entropy-driven, emergent behavior. (vi) We demonstrate this design rule in simulations that allow particle shape to fluctuate dynamically by showing that when particles are constrained to sit on a target lattice, they spontaneously adopt their preferred shape; that is, the shape that minimizes the free energy of the target structure at a given state point.

Through all of these findings we demonstrate what the outlines of a periodic table of colloidal elements might look like. In particular, because colloidal valence is not constrained, a colloidal periodic table cannot be as succinct as the atomic periodic table. However, because colloidal valence can be manipulated, a colloidal periodic table can encode detailed, quantitative relationships between building block attributes and bulk behavior, and can tell us what building blocks are optimal for a given structure, and why they are optimal.

## I. THEORETICAL RESULTS

We consider a family of colloidal elements that can be described by a set of isotropic interaction potentials, or by anisotropy dimensions for enthalpic [8] or entropic [14] patches, with parameters  $\{\alpha_i\}$ . The particles are described by a classical Hamiltonian  $H$  that depends on the  $\alpha_i$  via a pair interaction between particles, and the rotational kinetic term in the Hamiltonian

$$H(\{\alpha_i\}) = \frac{p^2}{2m} + \frac{1}{2}L^T I_{\{\alpha_i\}}^{-1} L + U_{\{\alpha_i\}}(q, Q), \quad (1)$$

where  $p$  are momenta,  $L$  are angular momenta,  $I$  is the moment of inertia tensor, and  $U$  is the interaction potential that depends on particle positions  $q$  and orientations  $Q$ , and where we have suppressed particle indices. We consider systems in which the generalized particle coordinates and their conjugate momenta do not have explicit dependence on the  $\alpha_i$ . In this case, the  $\alpha_i$  have vanishing Poisson brackets with the Hamiltonian, and are invariants of the system:  $\{\alpha_i, H\} = 0$ . This is the case if, *e.g.*, a particle's shape is independent of its generalized momentum and position. This would not hold, *e.g.*, for systems with chemical gradients that cause a particle to swell in some locations more than others. Furthermore, we consider systems in which the  $\alpha_i$  themselves are mutually commuting, *i.e.*, the order in which operations are applied to modify the building blocks is not important. We regard the  $\alpha_i$  as a set of mutually conserved charges, and it has been shown [44, 45] that there is a well-defined thermodynamic ensemble for any set of mutually commuting conserved charges.

Formally, we consider a system where the  $\alpha_i$  fluctuate thermally about some averages  $\langle \alpha_i \rangle$ , and the energy fluctuates about an average  $\langle E \rangle$ . The partition function for this ensemble

can be found with various methods. For brevity we start with the Shannon/Jaynes [46, 47] entropy

$$S = - \sum_{\sigma} \left[ \pi_{\sigma} \ln(\pi_{\sigma}) - \beta \left( \pi_{\sigma} H - \langle E \rangle - \sum_i \mu_i N (\pi_{\sigma} \alpha_i - \langle \alpha_i \rangle) \right) \right], \quad (2)$$

where we have set  $k_B = 1$ ,  $\pi_{\sigma}$  is the probability of finding the system in a state labelled  $\sigma$ ,  $\beta$  and  $\mu_i$  are Lagrange multipliers enforcing the thermal averages,  $N$  is the number of particles in the system (the factor of  $N$  is included here so that both  $\mu_i$  and  $\alpha_i$  can be intensive quantities), and the summation should be interpreted schematically. Unless otherwise noted we will work in units where the particle volume  $\ell^3 = 1$ . To determine the partition function we maximize Eq. (2) with respect to  $\pi_{\sigma}$ . This gives, up to some normalization constant  $\mathcal{Z}$ ,

$$\pi_{\sigma} = \frac{1}{\mathcal{Z}} e^{-\beta(H - \sum_i \mu_i N \alpha_i)}, \quad (3)$$

and fixing the normalization  $\sum_{\sigma} \pi_{\sigma} = 1$  gives

$$\mathcal{Z} = \sum_{\sigma} e^{-\beta(H - \sum_i \mu_i N \alpha_i)}. \quad (4)$$

We see that  $\beta = 1/T$ , the usual inverse temperature, and  $\mu_i$  are generalized chemical potentials conjugate to the ‘‘charges’’  $\alpha_i$  [45] that determine the building block attributes. To distinguish  $\mu_i$  from the ordinary chemical potential, and since they act as sources for changing the ‘‘elemental’’ building blocks of the system, we refer to them as ‘‘alchemical’’ potentials. We define the thermodynamic potential for this ensemble as  $\mathcal{Z} \equiv e^{-\beta\phi}$ , which gives

$$\langle \alpha_i \rangle = -\frac{1}{N} \left( \frac{\partial \phi}{\partial \mu_i} \right)_{N, \eta, T, \mu_j \neq i}, \quad (5)$$

where  $\eta$  is the packing fraction or density. This computes how the system responds to a change in alchemical potential, and in the thermodynamic limit (hereafter we will be concerned about the thermodynamic limit so we will drop the  $\langle \rangle$  notation) establishes a constitutive relation  $\alpha_i(\eta, T, \{\mu_j\})$ . It is convenient to make a Legendre transformation  $F = \phi + \sum_i \mu_i N \alpha_i$ , and compute the constitutive relation  $\mu_i(\eta, \beta, \{\alpha_j\})$  using the expression

$$\mu_i = \frac{1}{N} \left( \frac{\partial F}{\partial \alpha_i} \right)_{N, \eta, T, \alpha_j \neq i}. \quad (6)$$

For notational simplicity, especially in cases where we consider a single  $\alpha_i$ , it will sometimes be convenient to drop the subscripts on  $\alpha$  and  $\mu$ .

The constitutive relation  $\mu(\alpha)$  quantifies the thermodynamic response of a system to a change in the attributes of the constituent particles. See appendix for a discussion of higher order thermodynamic response functions. If the alchemical potential  $\mu > 0$  at some state point  $NVT\alpha$ , then an infinitesimal increase in the alchemical parameter  $\alpha$  would increase

the free energy of the system. Conversely if  $\mu < 0$  then an infinitesimal increase in  $\alpha$  would decrease the free energy of the system. This has two important implications. (i) Locally optimal particle attributes  $\alpha^*$  are determined by the roots of the constitutive relation  $\mu(\alpha^*) = 0$  with positive slope. We show in appendix that the locations of these roots are invariant under reparametrizations of  $\alpha$ . (ii) In hard particle systems, where the free energy simply measures the system entropy,  $\mu$  directly measures how the number of states available to a system changes as a function of the particle shape, and so it can be used to systematically determine which particle features are most likely to come into contact, and provides explicit quantitative guidance on how to design shapes for structures. We demonstrate both of these implications below.

In the next section, we explicitly compute  $\mu$  in three example systems, and interpret the meaning and implications of each computation. We compute the constitutive relation  $\mu_i(\eta, T, \{\alpha_j\})$  at  $\eta, T, \{\alpha_j\}$  numerically using Eq. (6) with the Bennett acceptance ratio method [48]. Using this method, we compute  $\mu$  at some  $\{\alpha_j\}$  by equilibrating several independent samples at nearby values  $\alpha_j + \nu h_j$ , where  $\nu$  are constants chosen for an appropriate finite differencing scheme, and  $h_j$  are finite differences. For a full description of the computation, see appendix. To determine valence for anisotropic particles, we use the potential of mean force and torque (PMFT), as described in Ref. [16].

In addition to constitutive relations between thermodynamic quantities (*i.e.* first order derivatives of the free energy), physical systems are also frequently characterized by higher free energy derivatives: susceptibilities and moduli (see, *e.g.*, Refs. [49, 50]). We define the alchemical modulus  $M_\alpha$  and susceptibility  $\chi_\alpha$  as

$$M_\alpha \equiv \left( \frac{\partial \mu}{\partial \alpha} \right)_{N, \eta, T}, \quad \chi_\alpha \equiv \left( \frac{\partial \alpha}{\partial \mu} \right)_{N, \eta, T}. \quad (7)$$

The extension to systems with several alchemical parameters is straightforward. We note that, like standard moduli (*e.g.* bulk, shear, Young's),  $M_\alpha$  is a stress-strain relationship [50], but the strain is in alchemical space rather than real space. Accordingly, alchemical modulus  $M_\alpha$  Eq. (7) at  $\alpha^*$  measures how sensitive the system is to deviations from the ideal particle properties. Similarly, like standard susceptibilities (*e.g.* compressibility) [50],  $\chi_\alpha$  is a strain-stress relationship. Physically, *e.g.*, by the fluctuation-dissipation theorem (see, *e.g.*, Ref. [49])  $\chi_\alpha$  determines how quickly a system of, say, fluctuating shape relaxes when particles are perturbed from their equilibrium attributes.

## II. NUMERICAL RESULTS AND DISCUSSION

We use our digital alchemy methodology to optimize building blocks for self-assembly in three different case studies. The first two involve entropy-driven systems, which are among the most conceptually difficult in which to connect macroscopic and microscopic system properties because the macroscopic behaviors are intrinsically collective.[14, 16, 51–53] In the

third study, we investigate an oscillating pair potential, which was recently shown [42] to self-assemble a one-component icosahedral quasicrystal, one of the most complex crystal structures known. In each case, the details of the specific model are included in the discussion below. Details and extended discussion of the methods used in each case may be found in the SI.

### A. Truncated Tetrahedra

We simulated a one-parameter family of truncated tetrahedra at moderate truncations known to self-assemble diamond lattices [33]. We parametrized the truncation between  $\alpha = 0$  (a tetrahedron maximally truncated so that it is an octahedron) and 1 (an untruncated, regular tetrahedron). With this parametrization (we discuss reparameterization invariance of our results in appendix) particles self-assembled diamond at a packing fraction of  $\eta = 0.6$  between truncations of 0.25, and 0.475 (see Fig. 1a). For reference, the Archimedean truncated tetrahedron [33] has a truncation of  $\frac{1}{3}$ . We performed standard Monte Carlo simulations (*e.g.* Ref. [54]) of systems of  $N = 216$  and 1000 particles at fixed volume. Polyhedra overlaps were checked using the GJK algorithm [55].

For the truncated tetrahedra, we computed the constitutive relation between vertex truncation  $\alpha$  and its conjugate alchemical potential  $\mu$ . We first computed  $\mu$  in small systems of  $N = 216$  particles, and found preliminary evidence for vanishing alchemical potential (here, a free energy minimum) for  $0.35 < \alpha^* < 0.4$ , (Fig. 1d, squares). To obtain higher precision, and to test for finite size effects, we simulated systems of  $N = 1000$  particles in the region surrounding the putative free energy minimum (Fig. 1d, circles). From these alchemical potential computations we extracted the free energy of the system as a function of shape in the vicinity of the minimum (Fig. 1d, inset), which we estimated by performing a weighted least squares fit to

$$\beta\mu = \beta M_\alpha(\alpha - \alpha^*), \quad (8)$$

from which we find the free energy minimum is at

$$\alpha^* = 0.3736 \pm 0.0001, \quad (9)$$

and the alchemical modulus  $M_\alpha$  is

$$\beta M_\alpha(\alpha = \alpha^*, \eta = 0.6) = 52.0 \pm 0.3. \quad (10)$$

We also constructed diamond densest packings (Fig. 1f) for truncated tetrahedra for all truncations (in increments of 0.001) at which self assembly into diamond lattices was reported in Ref. [33], and find the curve has a maximum consistent with the Archimedean truncated tetrahedron at  $\alpha_A = 1/3$ .

To directly examine the effects of shape modification on emergent valence [14, 16], we computed the PMFT for systems of  $N = 1000$  truncated tetrahedra. For details of this computation, see Ref. [16]. We computed the PMFT at a density of  $\eta = 0.6$  for a truncation of  $\alpha = 0.25$  (Fig. 2a), and a truncation of  $\alpha^*$  (Fig. 2b). The results for the first neighbor

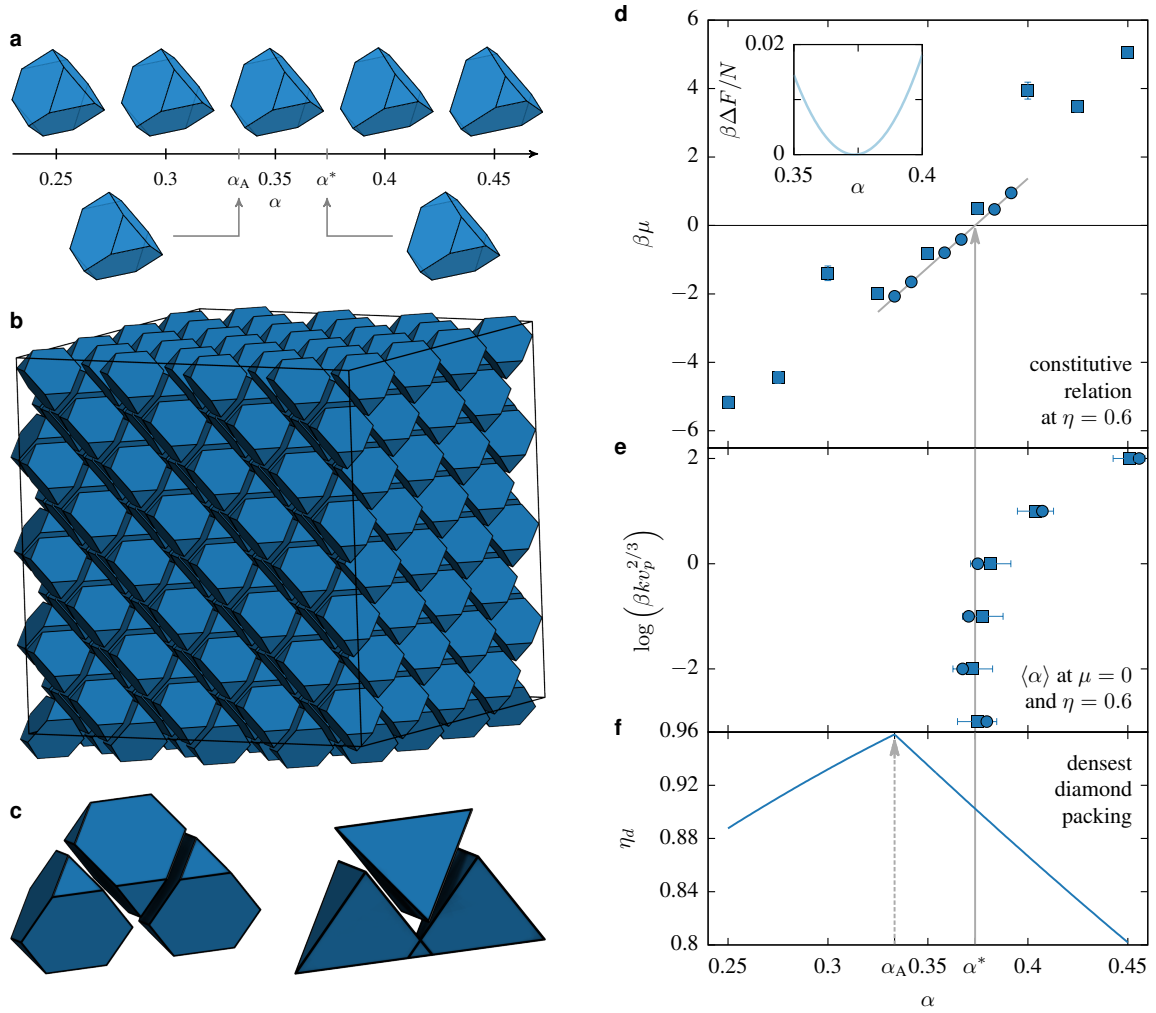


Figure 1. Truncated tetrahedra at a range of truncations  $\alpha$  (a) self-assemble a diamond lattice (b) [33]. A search for maximal diamond packing density,  $\eta_d$  (f) would suggest optimal assembly at  $\alpha_A = 1/3$ , the Archimedean truncated tetrahedron. We compute the constitutive relation (d)  $\mu(\alpha)$  (Eq. (6)) for hard truncated tetrahedra at  $\eta = 0.6$ . Squares (■) are results for systems with 216 particles, circles (●) for systems with 1000 particles; where visible, error bars are one standard deviation. The alchemical potential vanishes when the truncation is optimal for self-assembling diamond at this density when the truncation is approximately  $\alpha^* \approx 0.37$ . In the inset plot we reconstruct the free energy curve in the vicinity of the minimum. The increase in anisotropy  $\alpha^*$  above the geometric prediction  $\alpha_A$  arises because particles need to increase anisotropy to preserve tetrahedral valence at lower packing fractions, but if particles are too anisotropic, the simultaneous coordination of neighboring particles is sterically prohibited (c, see also Fig. 2). We demonstrate this design rule (e; see also appendix Movie) by simulating tetrahedra with fluctuating shape at  $\mu = 0$  in an Einstein crystal with spring constant  $k$  at packing fraction  $\eta = 0.6$  and allowing the particles to find their optimal shape. The plot (e) shows that at low  $k$  the average truncation  $\langle \alpha \rangle$  is consistent with  $\alpha^*$  ( $N = 216$  squares ■;  $N = 1000$  circles ●).

shell show particles have stronger tetrahedral valence at  $\alpha^*$  than at  $\alpha = 0.25$ , which originates from the relatively larger hexagonal faces acting as stronger entropic patches [14]. However, we see that at a fluid density of  $\eta = 0.5$ , in the second neighbor shell when particles have the optimal truncation  $\alpha^*$  (cyan spots in Fig. 2c), the next-to-nearest neighbors sit in an alternating arrangement, whereas the next-to-nearest neighbors for perfect tetrahedra (blue spots in Fig. 2d) are rotated by  $\pi/6$ . This indicates a non-alternating arrangement that coincides with polytetrahedral motifs not commensurate with the

diamond lattice, which arises from steric constraints depicted in Fig. 1c. To directly confirm this result, we performed simulations in an  $NVT\mu$  ensemble (*i.e.* both thermostated and “alchemostated”) to determine  $\alpha(\mu)$  at  $\mu = 0$  for  $N = 216$  and 1000 truncated tetrahedra with fluctuating shape in a diamond Einstein crystal. We initialized the system at low packing fraction  $\eta = 0.2$  with fully truncated (*i.e.* octahedral,  $\alpha = 0$ ) particles, and slowly compressed the system to the target packing fraction of  $\eta = 0.6$ , after which we relaxed the spring constant. We observed that the process drove the particles to

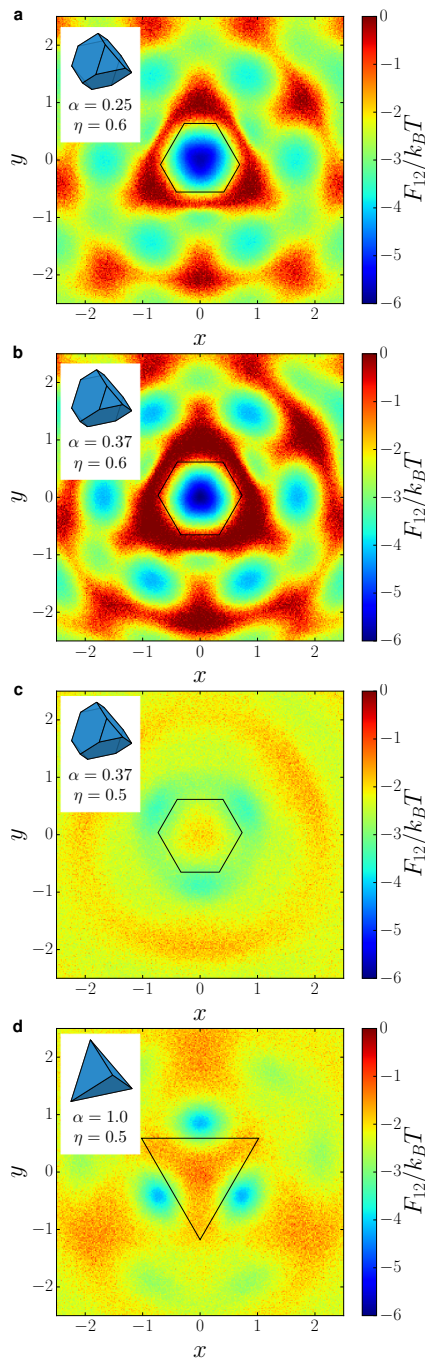


Figure 2. Emergent valence encoded in the PMFT for truncated tetrahedra for a crystal at density  $\eta = 0.6$  (a:  $\alpha = 0.25$ , b:  $\alpha = \alpha^* \approx 0.37$ ), and a fluid at density  $\eta = 0.5$  (c:  $\alpha = \alpha^* \approx 0.37$ , d:  $\alpha = 1.0$ ). In the crystal we see that the particle at the optimal truncation  $\alpha^*$  (b) shows greater specificity of tetrahedral valence than at lower  $\alpha$  (a), as expected. However, at fluid densities, we see that if the particle is too tetrahedral (d), the second neighbor shell is by  $\pi/6$  compared with lower truncations (c), and is incommensurate with the diamond lattice.

spontaneously adopt a truncation consistent with our alchemical potential calculations at fixed shape. See Fig. 1e, and

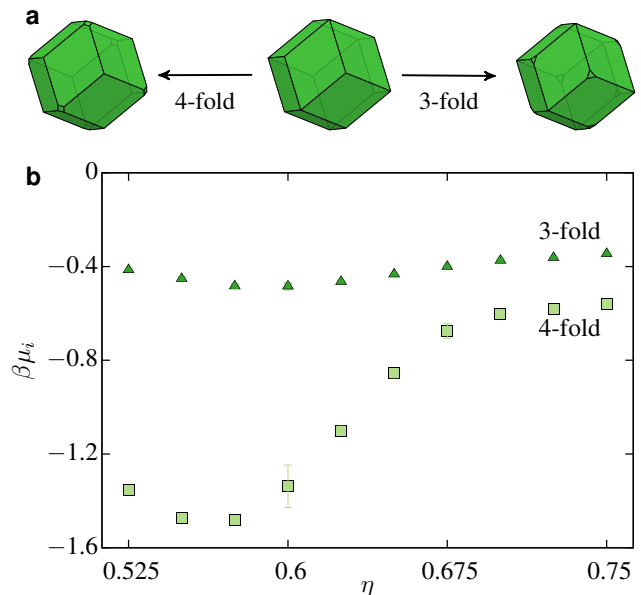


Figure 3. Rhombic dodecahedra have both four-fold and three-fold vertices (a). We determine the relative sensitivity to the truncation of each type of vertex by computing the constitutive relation  $\mu(\eta)$  (b) according to the (exaggerated) truncations shown in (a). We plot alchemical potentials for 4-fold truncations ( $\mu_4$ ,  $\square$  squares) and 3-fold truncations ( $\mu_3$ ,  $\triangle$  triangles) at various densities for which the system self-assembles an fcc lattice. We observed  $\mu_4 < \mu_3 < 0$  at all densities, indicating that both vertex truncations improve assembly of the target crystal, but four-fold vertex truncations provide greater improvement.

appendix movie.

Our computation of the constitutive relation  $\mu(\alpha)$  for truncated tetrahedra that form a diamond lattice reveals several findings. (i) By determining that  $\mu(\alpha)$  has a root at  $\alpha^* \approx 0.37$  we have demonstrated that it is possible to find a thermodynamically optimal shape, among a given family, for self-assembling the diamond lattice. (ii) Our criterion of  $\mu(\alpha^*) = 0$  is both parameter-free and independent of system kinetics, which are highly dependent on simulation methods. Nevertheless, we find rough agreement between the thermodynamic computation of the alchemical potential and a measurement of the lower critical packing fraction  $\eta_c$  reported in Ref. [33]. (iii) The fact that the optimal particle shape ( $\alpha^* \approx 0.37$ ) for diamond assembly at  $\eta = 0.6$  is more tetrahedral than the optimal shape for diamond packing ( $\alpha_A = 1/3$ ), but not perfectly tetrahedral ( $\alpha = 1$ ), arises from a competition between two effects. Particles must have tetrahedral valence to form the diamond lattice, but in the diamond lattice, particles are arranged in an alternating motif (Fig. 1c,d). Shape entropy considerations [16] suggest that as the system density is lowered, particles must have larger entropic patches [14] to maintain their emergent valence, as shown in Fig. 2. However, as illustrated in Fig. 1d, if the particles are too tetrahedral, then the alternating diamond motif leads to overlapping next-to-nearest neighbor particles, as shown in Fig. 2. Hence, the optimal truncation

of a tetrahedron to self-assemble diamond is more tetrahedral than packing would dictate to preserve valence, but not too tetrahedral to prevent particles from having alternating valence. (iv) We computed the alchemical modulus  $M_\alpha$  for truncated tetrahedra at  $\eta = 0.6$  and  $\alpha = \alpha^*$ . In future work it would be interesting to determine how this modulus varies across system density in this system and differs between systems/structures, or relates to effects of polydispersity, and how it behaves at phase boundaries. (v) The entropic assembly of anisotropic hard shapes is driven by emergent valence[14, 16], manifesting in directional entropic forces[33]. A defining feature of emergent behaviors is that their origin is difficult to trace to microscopic attributes of the system constituents.[17] Here, we explicitly demonstrate the general principle that it is possible to optimize building block attributes, by which we systematically control emergent valence, in order to optimally assemble a target structure. Moreover, our results suggest a general design rule for entropic valence: that as system density decreases, entropic patch size [14] must increase to optimally assemble a dense packing phase. This design rule is supported by another recent result [43] where it was found that for several families of dimpled particles, the peak in packing density occurs at an entropic patch size that is below the critical size for the *onset* of entropic assembly at low density. This is particularly strong evidence for the design rule proposed here because the optimal patch size cannot be smaller than the patch size at onset. (vi) In practice, the synthesis of anisotropic colloidal particles is often driven by a growth process that yields particles in a family of shapes. Here we have shown, in an example family, how to optimally choose when to terminate that growth process to obtain particles for assembling a specific target structure.

## B. Rhombic Dodecahedron

To (i) understand how to contrast the relative importance of different shape modifications of a given shape, and (ii) determine how this relative importance depends on system density, we studied a two-parameter family of truncations of rhombic dodecahedra that leave them invariant under the spheric triangle group  $\Delta_{4,2,3}$ . [56] The  $\Delta_{4,2,3}$  invariant family of shapes is constructed with three families of planes that make up the faces of a cube, a rhombic dodecahedron, and an octahedron, all oriented to preserve the necessary point group symmetry. The rhombic dodecahedron has two different types of vertices: four-fold vertices where four planes come together, and three-fold vertices where three planes come together. Moving the planes that make up the faces of the cube towards the origin truncates the four-fold vertices, and moving the planes that make up the faces of the octahedron truncates the three-fold vertices. We performed simulations that examine the effects of each type of truncation on a perfect rhombic dodecahedron. We parametrize the vertex truncations so that when  $\alpha_4 = 0$  (four-fold vertex truncation) and  $\alpha_3 = 0$  (three-fold vertex truncation) the particle is a perfect rhombic dodecahedron. Maximal truncation  $\alpha_4 = 1$  and  $\alpha_3 = 0$  yields a perfect cube, and  $\alpha_4 = 0$  and  $\alpha_3 = 1$  yields a perfect octahedron.

We determined how systems of perfect rhombic dodecahedra

( $\alpha_4 = \alpha_3 = 0$ ) respond to infinitesimal changes in  $\alpha_3$  and  $\alpha_4$ . We computed the alchemical potentials  $\mu_4$  conjugate to  $\alpha_4$  (four-fold vertex truncations) and  $\mu_3$  conjugate to  $\alpha_3$  (three-fold vertex truncations) for systems of  $N = 256$  rhombic dodecahedra at a series of packing densities  $\eta$  between 0.525 and 0.75 in increments of 0.025 at  $\alpha_4 = \alpha_3 = 0$ . As shown in Fig. 3 we find negative alchemical potentials for both 3-fold and 4-fold vertex truncations ( $\mu_3, \mu_4 < 0$ ) at all densities studied  $0.525 \leq \eta \leq 0.75$ , implying that both types of vertex truncation *reduce* the free energy of the system. Moreover, we find that truncation of the four-fold vertices results in a greater reduction in free energy than the three-fold truncation.

Our computation of the constitutive relations  $\mu_i(\eta)$  for rhombic dodecahedra explicitly demonstrates how our methods can determine the relative importance of various shape features. Determining the most important shape features to control is crucial for anisotropic particle synthesis techniques, and here we have demonstrated a general method for solving this problem. In addition to providing this general proof-of-principle, our results have several specific implications. (i) At all densities studied, we observed  $\mu_4 < \mu_3 < 0$  indicating that both types of vertex truncation improve the self-assembly of rhombic dodecahedra into a face-centered cubic (fcc) lattice. Because vertex truncation at fixed volume means the particles become slightly more spherical, our result suggests that the structure is further stabilized by particles exchanging some vibrational degrees of freedom for rotational ones. Moreover, (ii) because  $\mu_4 < \mu_3$  it suggests that the four-fold vertex truncations are more important in restricting the rotational motion than the three-fold vertices. There are 8 three-fold vertices and 6 four-fold vertices in a rhombic dodecahedron, but the centroid-to-vertex distance for a four-fold vertex is  $4/3$  the distance for a three-fold vertex. We might suspect that if a vertex sticks out further from the shape, or is greater in number, it will provide a greater steric constraint on the microstates available to the system. Our result that  $\mu_4 < \mu_3$  suggests that for the rhombic dodecahedron in an fcc lattice, the vertex distance is more important than the number of vertices. It would be interesting to investigate whether this design rule holds for other shapes, or is specific to rhombic dodecahedra. (iii) Because the slopes of both  $\mu(\eta)$  curves are positive for  $\eta \gtrsim 0.6$ , it suggests that particles give up rotational entropy faster than translational entropy as the system density increases. We note that the distinction between four-fold and three-fold vertices becomes smaller at larger packing fractions, which suggests, surprisingly, that as the particles increasingly lose rotational entropy the distinction between *how* they lose it becomes *less* important. It would be interesting to see if this result holds more generally in other systems.

## C. Oscillating Pair Potential

To demonstrate that our alchemy approach is not limited to particle shapes, we studied spherical nanoparticles (or point particles) interacting isotropically using a truncated, intermediate range oscillating pair potential studied in [42], which is



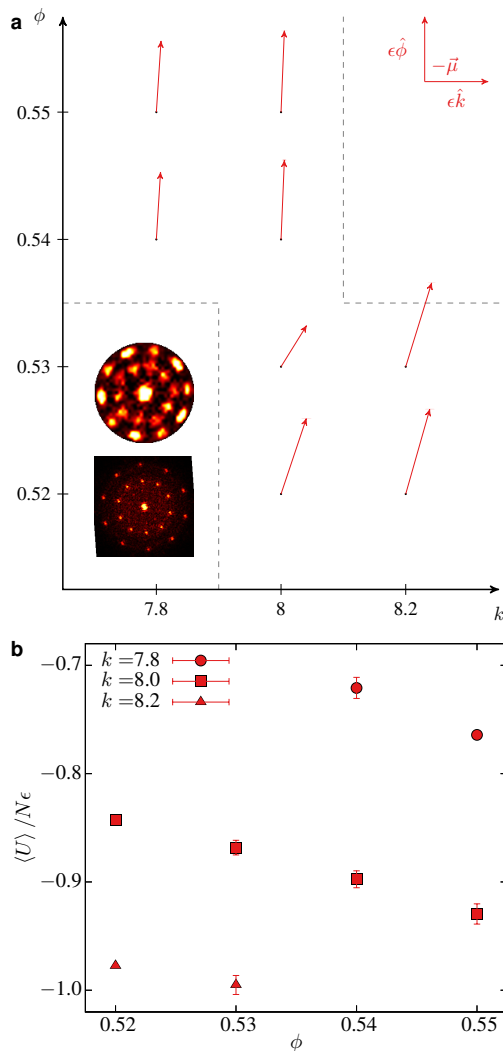


Figure 4. Panel a: Alchemical potential ( $-\vec{\mu}$ ) for the wavenumber  $k$ , and phase  $\phi$  parameters systems of  $N = 4096$  particles interacting *via* a three-well oscillating pair potential over a range of parameters that self-assemble an icosahedral quasicrystal.[42] The pair potential self-assembles icosahedral quasicrystals of three different densities. Here, we examine the region of parameter space that self-assembles the intermediate density quasicrystal (dashed lines indicate the phase boundaries we observed for the self-assembly of the intermediate density quasicrystal). Surprisingly, we find that, over the range of parameters we studied, in order to thermodynamically improve the assembly of the intermediate density quasicrystal, we are driven toward the region of parameter space that is dominated by the self-assembly of the high-density quasicrystalline phase. This suggests that the optimal choice of parameters to stabilize the intermediate density quasicrystal is buried in a region that will spontaneously self-assemble the high density phase instead, and suggests that the intermediate density phase will be difficult to stabilize in practice. The insets show the bond order diagram and diffraction pattern from a simulation snapshot of a 4096 particle system at  $k = 8, \phi = 0.53$ . Panel b: In the same system we computed the average potential energy per particle for different values of  $k$  as a function of  $\phi$ . We see a clear decrease in  $\langle U \rangle$  with increasing  $k$  and  $\phi$ . This finding suggests that the decrease in free energy with increasing  $k$  and  $\phi$  shown in panel a can be attributed to enthalpic contributions from lower ground state energies.

inspired by Friedel oscillations. It can be written in the form

$$U(r) = \frac{\epsilon}{r^{15}} + \frac{\epsilon}{r^3} \cos(k(r - 1.25) - \phi). \quad (11)$$

This potential has been recently shown to self-assemble an icosahedral quasicrystal for  $k_B T = 0.25$  for  $0.78 \lesssim k \lesssim 0.82$  and  $0.52 \lesssim \phi \lesssim 0.55$  [42]. The potential is of particular interest due to the possibility of realizing it in systems of nanoparticles or colloids decorated with appropriate ligands. For these computations, we work in units with  $\epsilon = 1$ . We performed simulations of  $N = 4096$  particles using HOOMD-Blue.[57] For full simulation details, see appendix.

We computed the alchemical potentials  $\mu_k$  conjugate to  $k$  (wavenumber) and  $\mu_\phi$  conjugate to  $\phi$  (phase shift) for systems of  $N = 4096$  particles interacting *via* the oscillating pair potential in Eq. (11). We studied the pair potential in the range of parameter space that was shown previously [42] to self-assemble an intermediate density icosahedral quasicrystal. In this phase, we find that within the entire parameter range over which we were able to reliably nucleate the intermediate density quasicrystal, both  $\mu_k$  and  $\mu_\phi$  are negative. We show this explicitly in Fig. 4a where we form  $\mu_k$  and  $\mu_\phi$  into the vector  $\vec{\mu}$ . We plot  $-\vec{\mu}$ , which shows the direction that decreases the free energy at a given point in parameter space.

This result alone does not indicate whether this curious behavior is enthalpic or entropic in origin. To understand the origin of this decrease in free energy for increasing both  $k$  and  $\phi$ , we computed the average potential energy at each state point, which is plotted in Fig. 4b. We see that at a given  $k$ , increasing  $\phi$  decreases the system's potential energy, and that the potential energy is lower at a given  $\phi$  with increasing  $k$ , which is consistent with the alchemical potential results shown in Fig. 4a. This suggests that the effect we observe in Fig. 4a is enthalpic in origin.

Surprisingly, our result that  $\mu_k$  and  $\mu_\phi$  are everywhere negative suggests that there is not a choice of parameters for which  $\vec{\mu} = 0$  (*i.e.* a local free energy minimum) in the parameter regime where the intermediate density quasicrystal is the thermodynamically preferred phase. (For an example of a simpler case where there is a local free energy minimum in a system with isotropic interactions, see appendix.) Rather it suggests that, at least for systems of  $N = 4096$  particles, the optimal parameter choice for self-assembling the intermediate density quasicrystal lies along the boundary separating the assembly of the intermediate density quasicrystal and the high density quasicrystal, which is the thermodynamically preferred phase at higher values of  $k$  and  $\phi$ . [42]

A general take-away message of Ref. [42] is that controlling assembly in one-component systems via isotropic interaction potentials involves two things. It involves controlling the relative distances of potential energy minima, which determines preferred relative distances between particles. Note that precise control over this procedure not straightforward, even at  $T = 0$ . See appendix for an explicit demonstration in a toy model system. However, it also involves controlling the relative depth of the minima, which determines the number of particles that sit at the preferred relative distances determined by the minima locations. Here, we are able to directly compute the effects

	Atomic Matter	Colloidal Matter
Anisotropy Dimensions	Proton Number	Many
Anisotropy Dimension Types	Discrete	Discrete, Continuous
Valence Constraints	Quantum Mechanics, Group Theory, Fermi Statistics	Steric
Number of Stable Elements	$\sim 80$	Infinite

Figure 5. Contrast between constraints on engineering materials with atomic elements and colloidal “elements”. Colloidal elements have valence that can vary continuously in many different ways. The malleability of colloid valence means that constructing a “periodic table” for them is inherently difficult. However, we can exploit the malleability of colloids to directly probe how particle attributes affect structure.

of changes in potential control parameters on the system free energy and we find that they can be detected. In appendix, we consider the pattern registration as measured by comparing the locations of the potential minima with the radial distribution function of the particles, and we find no discernible difference across the range of parameters we considered. This suggests that our alchemical potential methods are sensitive to system behavior that is not easily discernible *via* conventional analysis. We believe this might be of particular value in systems such as the oscillating pair potential system where there is a very rich bulk phase structure that depends sensitively on the choice of potential parameters controlling particle valence [42].

### III. CONCLUDING REMARKS

We chose families of model systems to demonstrate the power of our methods because of their structural complexity (the icosahedral quasicrystal), or conceptual complexity (the emergent behavior of hard shapes); however our methods can be generalized straightforwardly to systems of particles with other interactions or shapes, as well as systems with enthalpic patches [7–9] or multiple particle species. Furthermore, though our focus was on understanding macroscopic colloidal behavior within a given region of phase space, our methods can be applied to the crystallization of other types of matter, *e.g.* polymers, and the study of phase boundaries. One example where both are relevant is in the investigation of the polymorphism [58] or supramolecular isomerism in crystals of small molecules, which is relevant for pharmaceutical applications [59].

Here we focused on solving the problem of determining optimal building block attributes for target structures among a range of building blocks, from which we were able to extract design rules for emergent behavior. As a result, most of our calculations were of the constitutive relation  $\mu(N, V, T, \alpha)$ . However, for truncated tetrahedra we also considered (Fig. 1e and appendix Movie) the constitutive relation  $\alpha(N, V, T, \mu)$

for particles fixed to sit on a diamond lattice using a simple extension of Eq. (2) (see appendix for details). All of the foregoing discussion concerning interpretation of alchemical potentials, including the relation to building block optimality, continues to hold, where any quantities computed in extended ensembles are, by design, conditional on the externally imposed criteria. Using extended ensembles, it is straightforward (see appendix for details) to use our techniques for the discovery of building blocks for bulk materials given a suitable choice of external design criteria. We leave a full numerical investigation of this class of problems to future work.

Our method for determining optimal building blocks to self assemble target structures was based on the desire to make quantitative connections between building block attributes and bulk behavior. To make our proof-of-principle demonstration explicit, we ensured that the local minima we identified were *bona fide* global minima by computing exhaustively over relevant building block attributes. Rather than compute exhaustively as we have here, future investigations should reduce computational effort by employing global optimization techniques. Indeed, work aimed at optimizing building blocks for bulk attributes has employed genetic or evolutionary algorithms [60–64], or gradient descent [65]. Those approaches are complementary to the optimization part of the present work in three ways: (i) Our approach provides a systematic, rigorous, first-principles method for constructing probability distributions needed to apply the gradient descent method proposed in Ref. [65]. (ii) Genetic and evolutionary algorithms are powerful techniques that use external fitness criteria to perform non-local optimization. Our approach supplements these non-local approaches by providing direct, precise measurement of the physical response of a system to a local change in the attributes of building blocks. (iii) The ability to probe local changes in building block attributes is also important because, in addition to optimizing attributes, we would like to be able to derive generalizable design rules that extend beyond specific systems of interest. Here we showed an example of how to accomplish this using digital alchemy by showing that dense packing arguments for anisotropic shapes can be extended to lower density by increasing the size of entropic patches. We believe that a combination of the methods we present here with existing techniques [60–63, 65] will provide a powerful tool set for materials design.

Finally, our digital alchemy method shows how to phrase a generic class of relationships between building block attributes and bulk behavior for colloidal materials. For colloids, the fact that valence can vary in many ways (sometimes continuously) along several different anisotropy dimensions [8, 14] means that it is not possible, even in principle, for a periodic table of colloidal elements to be as succinct as the atomic periodic table (see Fig. 5). However, like the atomic periodic table relates atomic valence to bulk behavior, we have shown that it is possible to relate colloid valence to bulk behavior. Indeed, because colloid valence is so malleable, we have shown that building block property–bulk behavior relationships for colloids can be quantitative in a way that is not possible for atoms. In effect, whereas quantum mechanics dictates that the atomic periodic table is complete and succinct, but heuristic, the outlines for a



periodic table of colloidal elements suggested by this work are that it is complex and many-dimensional, but also quantitative, and richly predictive.

*This document is an unedited Author's version of a Submitted Work that was subsequently accepted for publication in ACS Nano, copyright (c) American Chemical Society after peer review. To access the final edited and published work see DOI:10.1021/acsnano.5b04181.*

We thank K. Ahmed, J. Anderson, D. Beltrán-Villegas, J. Crocker, E. Eiser, D. Frenkel, O. Gang, L. Isa, D. Kofke, I. Kretzschmar, R. Newman, B. Schultz, K. Stebe, A. Sweeney, and J. Swift for helpful discussions and encouragement; C. Phillips for providing simulation code for the Lennard-Jones-Gauss system; M. Engel for providing simulation code for the polyhedra; J. Antonaglia for a careful reading of an early version of the manuscript; J. Dshemuchadse for helpful discussions and comments on the manuscript; P. Damasceno for helpful discussions, encouragement, and assistance with structure identification; and H. Jaeger for generously sharing a pre-publication version of Ref. [65]. This material is based upon work supported by, or in part by, the U.S. Army Research Office under Grant Award No. W911NF-10-1-0518, the DOD/ASD(R&E) under Award No. N00244-09-1-0062, and the Department of Energy under Grant No. DE-FG02-02ER46000. D.K. acknowledges funding by the FP7 Marie Curie Actions of the European Commission, Grant Agreement PIOF-GA-2011-302490 Actsa.

## Appendix A: Supplementary Theory and Methods

### 1. Moments of Inertia

Our calculation of the alchemical potential that determines the constitutive relation  $\mu_i(\{\alpha_i\})$  depends on the moment of inertia tensor of the system. To see this, we write the partition function for the ensemble with fixed  $\{\alpha_i\}$  as

$$Z(\{\alpha_i\}) \propto \int [dp][dL][dq][dQ] e^{-\beta H}, \quad (\text{A1})$$

where  $q$  are particle positions,  $Q$  are particle orientations,  $p$  are conjugate momenta,  $L$  are angular momenta, we have suppressed particle indices, and for simplicity we are working in an ensemble with fixed volume and number of particles. The following discussion is straightforward to extend to other ensembles.

Starting with Eq. (A1), we integrate over the momenta and angular momenta, which gives (in three spatial dimensions)

$$Z(\{\alpha_i\}) \propto \beta^{-3N} m^{3N/2} (\det(I_{\{\alpha_i\}}))^{N/2} \int [dq][dQ] e^{-\beta U_{\{\alpha_i\}}(q,Q)}. \quad (\text{A2})$$

For simplicity, we will concern ourselves with changes in alchemical parameters that leave the particle mass and volume invariant so that we are isolating the effects of changes in shape

only. Defining

$$e^{-\beta \tilde{F}} \equiv \int [dq][dQ] e^{-\beta U_{\{\alpha_i\}}(q,Q)}, \quad (\text{A3})$$

we have, up to irrelevant constants, the thermodynamic potential

$$\beta F = -\frac{N}{2} \log \det(I_{\{\alpha_i\}}) + \beta \tilde{F}. \quad (\text{A4})$$

We compute alchemical potentials by differentiating this expression with respect to the  $\alpha_i$ . Even if the particle mass and volume are fixed, the first term depends on the particle shape, and so we need to compute the moment of inertia tensor of our particles.

This term does not contribute to the computation of isotropic (spherical particles), however it is important for polyhedral particles. Our computation used four steps. (i) We compute the moments of inertia by identifying all of the faces of the polyhedron. (ii) We do a fan decomposition of the faces into triangles. (iii) We use the point at the origin with the triangulation of each of the faces to decompose the polyhedron into a set of tetrahedra. (iv) We use standard formulae to compute the inertia tensor of the tetrahedron.[66] We checked that our code was correct by using it to compute moments of inertia for several known shapes. As an additional check, all shapes we considered are invariant under triangle group symmetries. Via Schur's lemma (see, e.g. [67]), their moments of inertia tensors must be proportional to the identity matrix, and we checked that our code gave results consistent with this up to machine precision.

### 2. Numerical Evaluation of Alchemical Potential

To evaluate the contribution of the configuration integral,  $\tilde{F}$ , to the alchemical potential we use a variant of the Bennett acceptance ratio method.[48]

We evaluate the expression

$$\mu_i = \frac{1}{N} \frac{\partial F}{\partial \alpha_i} \quad (\text{A5})$$

using finite differences. For brevity, we will give formulae for a single  $\alpha$ ; the extension to multiple  $\alpha$  is straightforward. For some finite  $h$ , we estimate

$$\frac{\partial F}{\partial \alpha} \approx \frac{1}{h} \sum_{\nu} \gamma_{\nu} F(\alpha + \nu h) \quad (\text{A6})$$

where,  $\gamma_{\nu}$  and  $\nu$  are appropriate constants for some finite differencing scheme [68]. To suppress numerical errors we used a symmetric four-point scheme for calculations involving truncated tetrahedra, the oscillating pair potential, and the 2D Lennard-Jones-Gauss system (see below); for rhombic dodecahedra we used a one-sided four point scheme.

For each state point  $\alpha$ , we independently equilibrated several copies of the target crystal lattice at each nearby  $\alpha_{\nu} = \alpha + \nu h$ . For the  $N = 216$  ( $h = 4 \times 10^{-4}$ ) systems of truncated

tetrahedra, the  $N = 4096$  oscillating pair potential systems ( $h_k = 3 \times 10^{-5}$ ,  $h_\phi = 10^{-5}$  or  $2 \times 10^{-5}$ ), and the  $N = 1024$  ( $h = 10^{-5}$ ) systems of Lennard-Jones-Gauss particles we self-assembled crystals from the fluid; for the  $N = 1000$  ( $h = 10^{-4}$ ) systems of truncated tetrahedra and the  $N = 256$  systems of truncated rhombic dodecahedra ( $h = 2 \times 10^{-3}$ ) we constructed the crystal directly. Without loss of generality, we labelled a particular  $\nu$  as  $\nu_0$ . For the hard truncated tetrahedra and rhombic dodecahedron systems, for all  $\nu \neq \nu_0$  we repeatedly sampled states from the equilibrium distribution using standard Metropolis Monte Carlo techniques (see, *e.g.* [54]), and computed the probability, according to the Metropolis criterion [69], of accepting a trial Monte Carlo move of the state from the ensemble with  $\nu$  to the ensemble with  $\nu_0$ . Similarly, we repeatedly sampled states from the equilibrium distribution of the system at  $\nu_0$ , and computed the probability, according to the Metropolis criterion, of making a trial Monte Carlo move of the state from ensemble  $\nu_0$  to each of ensembles at the other  $\nu$ . For the oscillating pair potential and Lennard-Jones-Gauss systems, we repeatedly sampled configurations from equilibrium  $NVT$  molecular dynamics trajectories coupled to a Langevin thermostat in HOOMD-Blue.[57] At each sample point we computed the potential energy in the system at a given  $\nu$  as well as what the potential energy would be if the particles maintained all of their positions but interacted with a potential  $\nu'$ . By recording these potential differences we constructed the probability, according to the Metropolis criterion, of making a Monte Carlo move from one value of  $\alpha$  to another.

To show how this computes the alchemical potential, we note that combining Eq. (A5) with Eq. (A6) and exponentiating we have

$$e^{-hN\beta\mu} \approx e^{-\sum_\nu \alpha_\nu \beta F(\alpha + \nu h)} = \prod_\nu e^{-\gamma_\nu \beta F(\alpha + \nu h)}. \quad (\text{A7})$$

Decomposing the thermodynamic potential into the kinetic and configuration components using Eq. (A4) we have

$$e^{-hN\beta\mu} \approx \prod_\nu e^{\gamma_\nu [\frac{N}{2} \log \det I(\alpha + \nu h) - \beta \tilde{F}(\alpha + \nu h)]}. \quad (\text{A8})$$

We then use detailed balance to write the configurational part of the free energy  $\tilde{F}$  at  $\alpha + \nu h$  in terms of the value at  $\alpha + \nu_0 h$  to get

$$e^{-hN\beta\mu} \approx \prod_\nu e^{\gamma_\nu [\frac{N}{2} \log \det I(\alpha + \nu h) - \beta \tilde{F}(\alpha + \nu_0 h)]} \left( \frac{p(\alpha + \nu_0 h | \alpha + \nu h)}{p(\alpha + \nu h | \alpha + \nu_0 h)} \right)^{\gamma_\nu}. \quad (\text{A9})$$

where  $p$  are the relevant transition probabilities we compute with the Bennett acceptance ratio method. We note that, since we are evaluating a first derivative of  $F$ ,  $\sum_\nu \gamma_\nu = 0$  so that

$$e^{-hN\beta\mu} \approx \prod_\nu e^{\gamma_\nu \frac{N}{2} \log \det I(\alpha + \nu h)} \left( \frac{p(\alpha + \nu_0 h | \alpha + \nu h)}{p(\alpha + \nu h | \alpha + \nu_0 h)} \right)^{\gamma_\nu}. \quad (\text{A10})$$

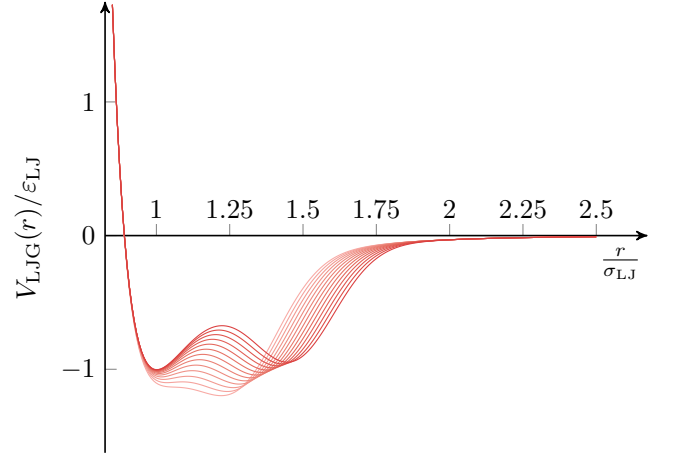


Figure 6. The functional form of the Lennard-Jones-Gauss potential (Eq. (C1)) for  $\epsilon_G/\epsilon_{LJ} = 3/4$ ,  $\sigma_G/\sigma_{LJ} = \sqrt{2}/10$ , and  $r_0/\sigma_{LJ}$  in the range for a two dimensional system to form a square lattice.

Finally, taking the logarithm of both sizes we get that

$$\beta\mu \approx \frac{1}{h} \sum_\nu \frac{\gamma_\nu}{2} \log \det I(\alpha + \nu h) - \frac{1}{Nh} \sum_\nu \gamma_\nu \log \frac{p(\alpha + \nu_0 h | \alpha + \nu h)}{p(\alpha + \nu h | \alpha + \nu_0 h)}. \quad (\text{A11})$$

Note that we did not attempt to determine general criteria for choosing optimal finite differencing schemes, *i.e.* the value of  $h$  or the order of the method. Two considerations that arise are that if  $h$  is too large, the finite differencing error is large, and a higher order method must be used. However, if  $h$  is too small, this affects the autocorrelation time of the transition probabilities which, necessitates more extensive sampling. Figuring out how to do this optimally for this type of computation is an interesting problem for future work.

### 3. Error Estimation

Numerical evaluation of the expression Eq. (A11) involves both systematic and statistical error. Statistical error comes from the estimation of the transition probabilities, and is given by

$$\delta(\beta\mu)_{\text{stat}} = \frac{1}{Nh} \sum_\nu \gamma_\nu \left( \frac{\delta p(\alpha + \nu_0 h | \alpha + \nu h)}{p(\alpha + \nu_0 h | \alpha + \nu h)} + \frac{\delta p(\alpha + \nu h | \alpha + \nu_0 h)}{p(\alpha + \nu h | \alpha + \nu_0 h)} \right). \quad (\text{A12})$$

Systematic error can arise from the calculation of the moment of inertia tensor. In practice, the moment of inertia tensor can be computed to machine precision, so this contribution is negligible. Further systematic error can arise if systems are equilibrated at slightly different densities. To see how

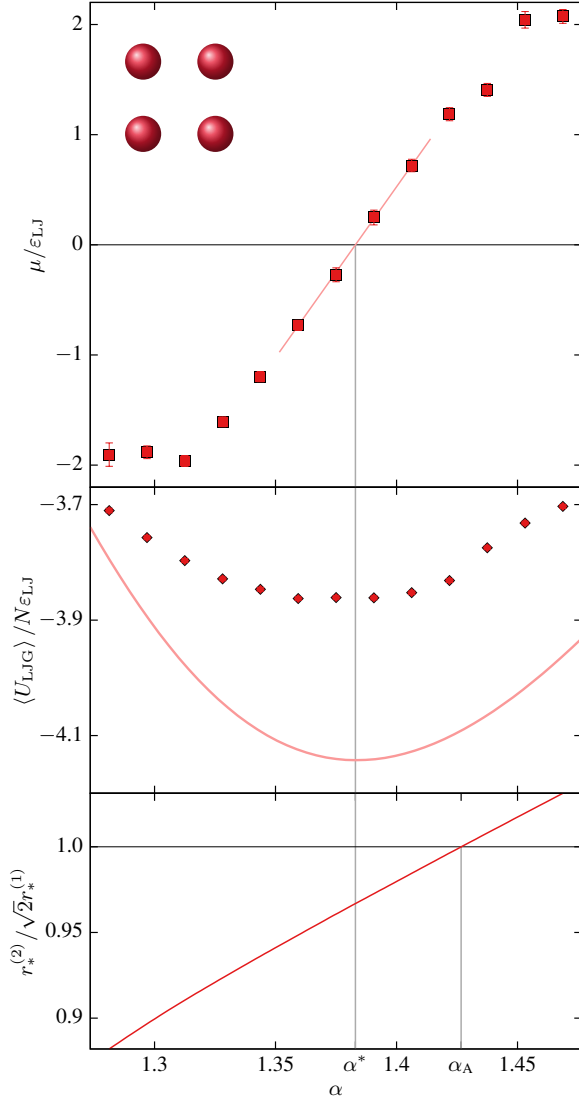


Figure 7. Constitutive relation  $\mu(\alpha)$  (■, top plot), where  $\alpha = r_0/\sigma_{LJ}$  describes the potential well position, for a two-dimensional Lennard-Jones-Gauss system of 1024 particles at  $k_B T = 0.1\epsilon_{LJ}$  (top). In this range of  $\alpha$  the system forms a square lattice. The alchemical potential vanishes at  $\alpha^* \approx 1.38$ , indicating that that is the optimal well-location for self-assembling a square lattice. This accords with a calculation showing that the potential energy is minimized at this well position both  $k_B T = 0.1$  (◆, middle plot) and at  $k_B T = 0$  (solid line, middle plot), but is lower than the naïve geometric estimate of that comes from pattern registration of the potential minima to the ratio of nearest-neighbor to next to nearest-neighbor distances in the square lattice ( $\sqrt{2}$ , intercept in lower plot).

this arises, consider the differential of the free energy for our systems, which has the form

$$dF = \mu N d\alpha - P dV. \quad (\text{A13})$$

where  $N$  is the number of particles, and for simplicity we are considering a single alchemical parameter  $\alpha$  and working in ensembles with fixed volume. To compute the alchemical

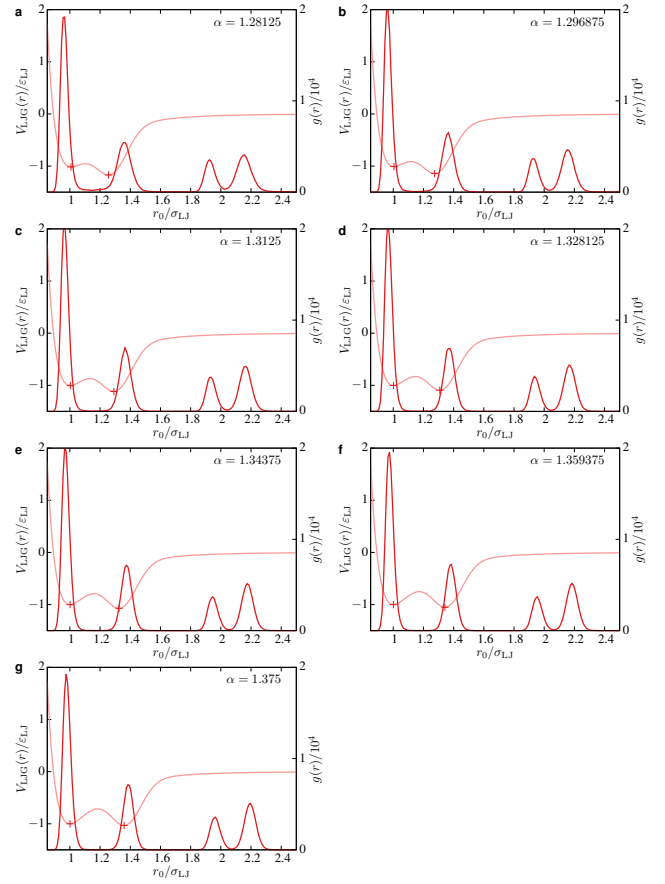


Figure 8. We examine pattern registration of self-assembled square lattices in 2D as shown through the radial distribution function ( $g(r)$ , darker curve) with the Lennard-Jones-Gauss pair potential (lighter curve, minima indicated with darker marks) that induces it to assemble, for various values of the parameter  $\alpha = r_0/\sigma_{LJ}$  (see Eq. (C1) in SI text). In these plots  $r_0$  is less than the critical value of  $\alpha^*$  where the alchemical potential  $\mu$  vanishes.

potential  $\mu$  we need to differentiate the free energy at fixed volume. However, there can be a variation in the system volume, which in our systems is reflected in a change in the packing fraction  $\eta$ , defined by

$$V = \frac{N\ell^3}{\eta}, \quad (\text{A14})$$

where  $\ell^3$  is the volume of a particle. Differentiating gives

$$dV = -\frac{N\ell^3}{\eta^2} d\eta. \quad (\text{A15})$$

So the differential for the free energy is given by

$$dF = \mu N d\alpha + \frac{NP\ell^3}{\eta^2} d\eta. \quad (\text{A16})$$

That means that to get a measurement of the alchemical potential, we need to have

$$\mu d\alpha \gg \frac{P\ell^3}{\eta^2} d\eta \quad (\text{A17})$$

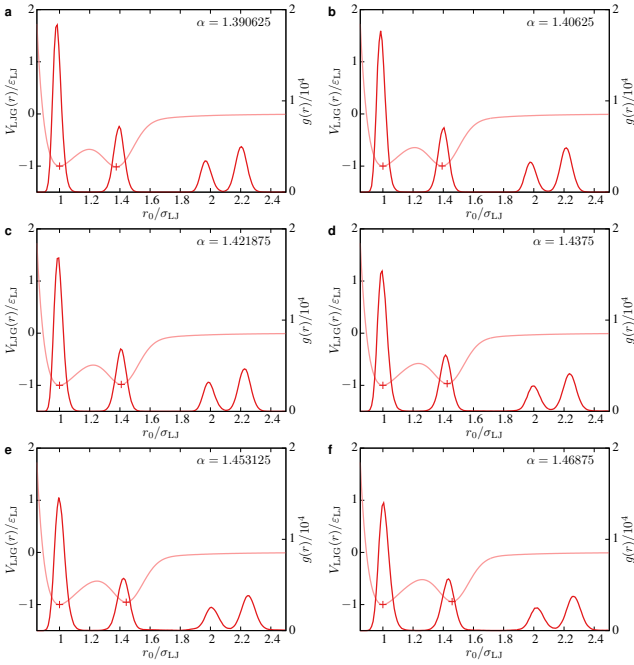


Figure 9. We examine pattern registration of self-assembled square lattices in 2D as shown through the radial distribution function ( $g(r)$ , darker curve) with the Lennard-Jones-Gauss pair potential (lighter curve, minima indicated with darker marks) that induces it to assemble, for various values of the parameter  $\alpha = r_0/\sigma_{LJ}$  (see Eq. (C1) in SI text). In these plots  $r_0$  is greater than the critical value of  $\alpha^*$  where the alchemical potential  $\mu$  vanishes.

to safely control the error arising from changes in packing fraction. We did this in two ways. For the systems of  $N = 1000$  truncated tetrahedra and  $N = 256$  rhombic dodecahedra we built perfect crystals at the desired packing fraction and then thermally equilibrated them. *E.g.* for the systems of  $N = 256$  rhombic dodecahedra, this fixes the variation in packing fraction to  $\lesssim 10^{-6}$ , and so the right hand side of Eq. (A17) is  $\sim 10^{-5}$ . On the left hand side  $d\alpha = 2 \times 10^{-3}$ , and  $\mu \sim 10^{-1}$ , which indicates that the spread in packing fraction contributes a systematic error on the order of 10%, which does not affect any of our conclusions. Systems of  $N = 1000$  tetrahedra are similar, but in that case we also find agreement between our alchemical potential computation and the computation with fluctuating shape (*c.f.* Fig. 2d,e, main text). For the systems of  $N = 216$  tetrahedra, we self-assembled crystals to within 1% of the desired packing fraction and then controlled for the errors in packing fraction statistically, and again the results of that computation agree with the computation with fluctuating shape.

For further confirmation, we note that our computation involves making trial moves between different types of particles in the same system. That means that when we compute the probability of going from  $\alpha \rightarrow \alpha + \delta\nu h$ , the volume of the system is invariant. And, similarly, when we compute the probability of going from  $\alpha + \delta\nu h \rightarrow \alpha$ , the volume is also invariant. However, there is a small difference in density *between* the two

systems. We tested controlling for this error in for four-fold vertex truncations at a density of  $\eta = 0.625$  where we observed since we observed the maximal sensitivity to packing fraction for that type of truncation at that density. We controlled for the error by independently equilibrating systems at packing fractions  $\eta_i$  distributed near the desired packing fraction  $\eta$ . We obtained a large number of independent samples of the transition probabilities for the various  $\eta_i$ . Given these transition probabilities, we used regression (weighted by the errors in each of the transition probabilities at  $\eta_i$ ) to estimate the value of  $p$  at  $\eta$ . We used the error from the regression estimate as the statistical error in  $\beta\mu$  in Eq. (A12). To well-within the error bounds we found no difference between the results obtained with densities randomly spread about the desired value, and those set to the desired value to machine precision.

#### 4. Numerical Limits on Determining Optimal Building Blocks

We note that in order to determine the roots of the constitutive relation  $\mu(\alpha)$  that determine optimal particle configurations to arbitrary accuracy runs up against the limit Eq. (A17). In practice we note that reasonable computations on modern hardware allow us to bound optimal shapes, for example, to differences in morphology that are imperceptible.

#### 5. Reparametrization and the Alchemical Constitutive Relation

Our calculations of optimal shapes and interactions for target structures were carried out by choosing a particular parametrization of the particle shape or interaction potential. This choice was not unique. For simplicity, consider a single parameter family of shapes or interaction potentials, and reparametrize them by  $\alpha = \alpha(\alpha')$ . Under this reparametrization, the constitutive relation becomes

$$\mu'(\alpha') = \frac{\partial\alpha}{\partial\alpha'}\mu(\alpha). \quad (\text{A18})$$

From this form we note that if the reparametrization is monotonic  $d\alpha'/d\alpha > 0$ , then  $\text{sgn}(\mu'(\alpha')) = \text{sgn}(\mu(\alpha))$ , which means that reparametrization will not change the direction of the change  $\alpha$  that corresponds to a decrease in free energy. Moreover, if  $d\alpha'/d\alpha \neq 0$ , any roots  $\alpha^*$  of the original constitutive relation  $\mu(\alpha) = 0$  will coincide with roots of the reparametrized constitutive relation  $\mu'(\alpha')$  according to  $\alpha'^* = \alpha'(\alpha^*)$ , which means that particle shapes, *e.g.*, determined to be optimal from our alchemical potential calculations are optimal regardless of the way in which particle shape is parametrized.

## Appendix B: Field Directed Alchemy: Design

### 1. Extended Ensembles

In the main text, we are concerned with optimizing among known building blocks for a target structure, so we began with Eq. (2) (main text) to derive and interpret unbiased statistical ensembles. In order to design building blocks for a structure for which we do not have a set of *a priori* candidates, it is necessary to modify Eq. (2) (main text) so that the statistical ensembles are biased to form a structure with a desired property. To make this explicit, we suppose there is some quantity  $\Lambda$  that when evaluated on the design structure takes the value  $\langle \Lambda \rangle$ . The ensemble for this system can be found by maximizing the entropy

$$S = - \sum_{\sigma} \left[ \pi_{\sigma} \ln(\pi_{\sigma}) - \beta \left( \pi_{\sigma} H - \langle E \rangle - \sum_i \mu_i N (\pi_{\sigma} \alpha_i - \langle \alpha_i \rangle) - \lambda (\pi_{\sigma} \Lambda - \langle \Lambda \rangle) \right) \right], \quad (\text{B1})$$

with respect to  $\pi_{\sigma}$ , where  $\lambda$  is a Lagrange multiplier. This yields the extended partition function

$$\mathcal{Z} = \sum_{\sigma} e^{-\beta(H - \sum_i \mu_i N \alpha_i - \lambda \Lambda)}. \quad (\text{B2})$$

Note that  $\lambda$ , which is a Lagrange multiplier, determines the strength of the coupling to the external field. We note that if  $\lambda$  is positive (negative), the system is driven toward particle configurations  $\alpha_i$  that favor increasing (decreasing)  $\Lambda$ , which allows one to design both toward or away from a structural characteristic encoded in  $\Lambda$ . Moreover, one could certainly use multiple structural characteristics with the aim of arriving at building blocks suitable for reconfigurable structures, or the suppression of some particular polymorph.

### 2. Fluctuating Shape: Detailed Balance and Interpretation

Here we show how to satisfy detailed balance in systems with fluctuating shape aimed at directly solving the problem of particle design. We begin with the generalized partition function from Eq. (B2)

$$\mathcal{Z} = \int d\alpha [dp][dL][dq][dQ] e^{-\beta(H - \mu N \alpha - \lambda \Lambda)}, \quad (\text{B3})$$

where we have now explicitly included the measures for the integration over the particle momenta  $p$ , angular momenta  $L$ , positions  $q$ , and orientations  $Q$ , and for notational simplicity we use a single anisotropy parameter (the generalized form is straightforward). Taking the Hamiltonian from Eq. (1) (main text), we perform the quadratic integrals over  $p$  and  $L$  to get

$$\mathcal{Z} \propto \int d\alpha [dq][dQ] (\det(I_{\alpha}))^{N/2} e^{-\beta(U_{\alpha} - \mu N \alpha - \lambda \Lambda)}, \quad (\text{B4})$$

up to irrelevant overall multiplicative constants. Detailed balance requires that for a Markov chain Monte Carlo integration to converge to Eq. (B4) the ratio of the probability of making a move from a shape  $\alpha_1$  to a shape  $\alpha_2$   $\Pi_{1 \rightarrow 2}$  to the probability of the reverse move  $\Pi_{2 \rightarrow 1}$  is equal to the ratio of probabilities of being in those states

$$\frac{\Pi_{2 \rightarrow 1}}{\Pi_{1 \rightarrow 2}} = \frac{\pi_1}{\pi_2}. \quad (\text{B5})$$

Using Eq. (B4) we have

$$\frac{\Pi_{2 \rightarrow 1}}{\Pi_{1 \rightarrow 2}} = \frac{(\det(I_{\alpha_1}))^{N/2} e^{-\beta(U_{\alpha_1} - \mu N \alpha_1 - \lambda \Lambda)}}{(\det(I_{\alpha_2}))^{N/2} e^{-\beta(U_{\alpha_2} - \mu N \alpha_2 - \lambda \Lambda)}}. \quad (\text{B6})$$

We performed simulations of truncated tetrahedra with fluctuating shape at zero alchemical potential  $\mu = 0$ , in an external field  $\Lambda$  that forces the particles to sit in an Einstein crystal with spring constant  $k$  (measured in units of  $k_B T / \ell^2$ ). Alchemical moves were performed at fixed particle position and orientation, which allows us to simplify Eq. (B6) to

$$\frac{\Pi_{2 \rightarrow 1}}{\Pi_{1 \rightarrow 2}} = \frac{(\det(I_{\alpha_1}))^{N/2}}{(\det(I_{\alpha_2}))^{N/2}} e^{-\beta(U_{\alpha_1} - U_{\alpha_2})}. \quad (\text{B7})$$

To satisfy detailed balance, we take the Metropolis [69] criterion as

$$\Pi_{2 \rightarrow 1} = \min \left( 1, \frac{(\det(I_{\alpha_1}))^{N/2}}{(\det(I_{\alpha_2}))^{N/2}} e^{-\beta(U_{\alpha_1} - U_{\alpha_2})} \right). \quad (\text{B8})$$

In Fig. 1e (main text) we report  $\alpha(\mu = 0)$  for truncated tetrahedra at a packing density of  $\eta = 0.6$  using an externally imposed field that puts the particles in an Einstein diamond crystal with spring constant  $k$ . We show that  $\alpha(\mu = 0)$  increases with  $k$  (*i.e.* particles become more tetrahedral for large  $k$ ). This result has two implications. (i) It shows that we can optimize particle shape not only for the diamond structure, but that we can optimize particle shape for a diamond structure at a fixed density with a stiffness that is determined by the stiffness of the Einstein crystal we impose externally. This suggests, more generally, that digital alchemy can optimize both structures and properties of structures. (ii) It shows that one effect of making particles more tetrahedral is that they form a diamond lattice that is more stiff at fixed density. At large spring constants we observed  $\alpha \approx 0.5$ , however, we failed to observe the spontaneous assembly of diamond lattices in our simulations at truncations that were this small. Moreover, our alchemical potential calculations show that as the vertex truncation of tetrahedra decreases past the optimal value, particles lose entropy in the diamond lattice. These two results together show that though it is possible to tune the stiffness of the crystal, which might be surprising because entropy is the only governing property in these systems, the range over which additional properties can be tuned while still ensuring spontaneous self-assembly is limited by kinetic factors.

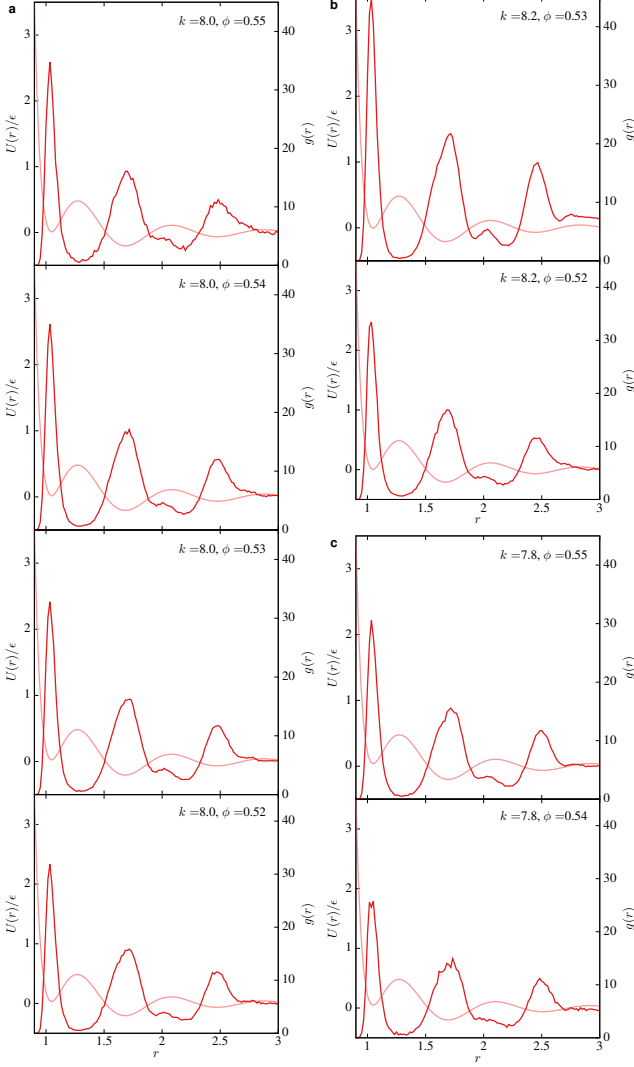


Figure 10. For the oscillating pair potential at fixed  $k$  (Panel a: 8.0, b: 7.8, c: 8.2) we show the pattern registration as measured by coincidence of peaks in the radial distribution function for a snapshot of the icosahedral quasicrystal ( $g(r)$ , darker curve), with the pair interaction potential ( $U(r, k, \phi)$ , lighter curve). We see no discernible difference in pattern registration over this range of parameters.

### Appendix C: Toy Model: Lennard-Jones-Gauss Potentials in 2D

As a consistency check, and as a non-trivial check on our analysis routines, we apply them to a system for which we can determine optimal microscopic parameters for the a given macroscopic state through direct calculations.

We study the effects of a one-parameter deformation of the relative position of potential minima in 2D Lennard-Jones-Gauss systems [24] *via* molecular dynamics simulations with HOOMD-Blue [57]. The potential is given by

$$V_{\text{LJG}} = \varepsilon_{\text{LJ}} \left( \left( \frac{\sigma_{\text{LJ}}}{r} \right)^{12} - 2 \left( \frac{\sigma_{\text{LJ}}}{r} \right)^6 \right) - \varepsilon_{\text{G}} e^{-(r-r_0)^2/2\sigma_{\text{G}}^2} \quad (\text{C1})$$

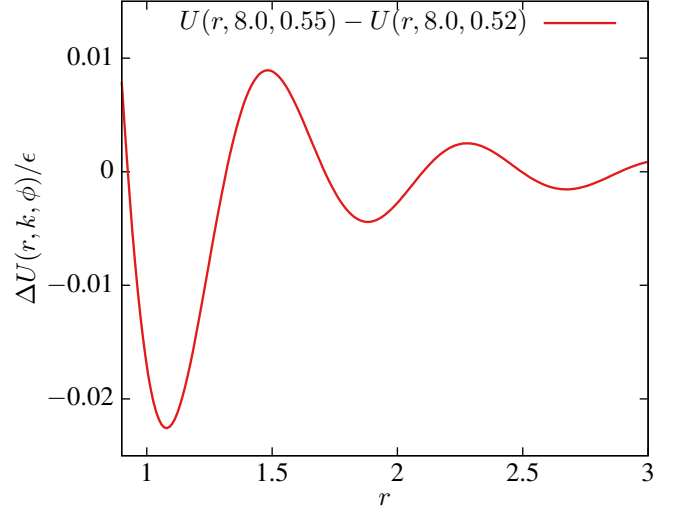


Figure 11. The variation in the oscillating pair interaction potential with  $\phi$  at fixed  $k = 8.0$  is small, yet leads to substantial gradients in the free energy (Fig. 4a, main text), and detectable differences in average potential energy per particle (Fig. 4b, main text), that are not discernible from the pattern registration depicted in Fig. 10a.

The phase diagram of this system has been previously determined in [24, 25]. We use potential parameters as in prior published work [25]:  $\varepsilon_{\text{G}} = \frac{3}{4}\varepsilon_{\text{LJ}}$  and  $\sigma_{\text{G}} = \frac{\sqrt{2}}{10}\sigma_{\text{LJ}}$ , and we work at  $T = \varepsilon_{\text{LJ}}/10$ . Finally, we define  $\alpha \equiv r_0/\sigma_{\text{LJ}}$ , and take it to be in the appropriate range to self-assemble a square lattice.

We studied the constitutive relation between  $\mu$  and  $\alpha \equiv r_0/\sigma_{\text{LJ}}$  for the Lennard-Jones-Gauss system in 2D. In Fig. 7 we plot the alchemical potential for a system of  $N = 1024$  Lennard-Jones-Gauss particles at  $T = 0.1\varepsilon_{\text{LJ}}$  for  $1.28125 \leq \alpha \leq 1.46875$  where we observed the formation of a square lattice. To determine the root of the constitutive equation, we performed a linear fit

$$\frac{\mu}{\varepsilon_{\text{LJ}}} \propto (\alpha - \alpha^*), \quad (\text{C2})$$

where we find  $\alpha^* = 1.383 \pm 0.001$ . For a square lattice, the ratio of the distance between first neighbours and second neighbours is  $\sqrt{2}$ . We numerically computed the locations of the minima of the Lennard-Jones-Gauss potential for  $r_0$  in the range where we observed formation of the square lattice, and found that ratio of the second minimum  $r_*^{(2)}$  to the first minimum  $r_*^{(1)}$  was  $\sqrt{2}$  when  $\alpha \approx 1.4267$ , which is well above the optimal value indicated by the alchemical potential calculation. Because the temperature is low, we expect the free energy to be dominated by the potential energy, so we computed the average potential energy, and found that there was a potential energy minimum between  $1.359375 \leq \alpha \leq 1.390625$  in agreement with our alchemical potential calculations.

Our alchemical potential calculation for the oscillating pair potential showed that it is possible to detect effects that are not readily apparent by examining the pattern registration between



$g(r)$  and the pair potential, as shown in Fig. 10. However, a surprising result of the computations for the Lennard-Jones-Gauss system in 2D is that even in simple cases where pattern registration effects are discernible, the optimal pattern registration is not what one would anticipate from naïve guessing.

In the Lennard-Jones-Gauss system, computations were performed at relatively low temperatures,  $T = 0.1\epsilon_{\text{LJ}}$ , and we would expect that at sufficiently low temperatures, the free energy of the system is dominated by the potential energy. In this case, we expect that the optimal  $\alpha^*$  we've determined above coincides with the value of  $\alpha$  with the lowest ground state energy. For the range of  $\alpha$  that self-assemble the square lattice, we compute the ground state energy as a function of both  $\alpha$  and the lattice spacing. For each  $\alpha$  we found the lattice spacing with the lowest energy to get the ground state energy of the square lattice as a function of  $\alpha$ . From this curve, we found the value of  $\alpha$  with the minimum ground state energy to be  $\alpha = 1.38342$ , which accords very well with the  $\alpha^*$  we computed using the alchemical technique at  $T = 0.1\epsilon_{\text{LJ}}$  (c.f. Fig. 7, top panel and middle panel). However, we note that Figs. 8 and 9 show the surprising result that neither result corresponds with the naïve ansatz of  $\alpha_A = 1.4267$  which that comes from fixing the relative distance between the first and second minima of the Lennard-Jones-Gauss potential  $r_*^{(2)}/r_*^{(1)} = \sqrt{2}$ , which we might expect to optimal because it coincides with the appropriate distances for the square lattice in 2D (see Fig. 7, lower panel). It is possible that this discordance between the naïve ansatz from pattern registration considerations, and the thermodynamically optimal pair potential might differ in other systems, which could be an important consideration in DNA-mediated nano-particle superlattice assembly.[70–80]

## Appendix D: Oscillating Pair Potential

### 1. Simulation Protocol

To evaluate the alchemical potentials conjugate to  $k$  and  $\phi$  for the oscillating pair potential system [42], we performed MD simulations of  $N = 4069$  particles using HOOMD-Blue [57], using a tabulated potential to directly reproduce the simulation technique employed in [42]. The system size of  $N = 4096$  particles was chosen so that sufficiently large changes in the  $k$  and  $\phi$  parameters of the potential could be made, and still replicate the simulation protocol followed in [42]. First, at each state point  $(k, \phi)$  we performed  $NVT$  simulations with a cooling schedule that was linear in temperature from an initial temperature of  $3\epsilon$  to  $0.525\epsilon$  over  $5 \times 10^7$  time steps, and then further from  $0.525\epsilon$  to  $0.25\epsilon$  over  $5 \times 10^7$  more time steps, to reach a supercooled fluid. From the supercooled fluid snapshots, we launched several  $NVT$  simulations to nucleate the quasicrystal, in each case seeding the random number generator of the Brownian integrator with a different integer. As

a consistency check we determined that on the boundaries of the stable range for the intermediate density quasicrystal we observed a substantial fraction of events in which we observed the nucleation of structures consistent with low density or high density quasicrystal where appropriate, which suggests that due to Lyapunov instabilities, our procedure leads to uncorrelated bulk structures over the whole range. We allowed each simulation to run for up to  $3 \times 10^8$  time steps, checking the potential energy every  $10^6$  time steps. Based on empirical criterion of  $U/N\epsilon < 0.25$  we determined that the quasicrystal had nucleated or was about to nucleate, and then ran the simulation for a further  $5 \times 10^6$  time steps. For each putative nucleated quasicrystal, we examined the structure and compared it with the structures reported in [42]. Note that, likely due to the relatively small number of particles ( $N = 4096$ ) we found the region of self-assembly of the intermediate density quasicrystal was smaller than that reported based on simulations of larger systems in [42]. For each intermediate density quasicrystal, we equilibrated for  $1.3 \times 10^8$  time steps, and then over a period of  $1.2 \times 10^8$  time steps we stored a snapshot of the system every  $4 \times 10^6$  time steps. All of the above time scales were determined to ensure decorrelation based on autocorrelation measurements of the potential energy, and observing diffusion of the quasicrystal in the simulation box. From these many independent samples of the structure at a given  $(k, \phi)$ , we randomly selected snapshots to re-equilibrate at nearby  $(k', \phi)$  or  $(k, \phi')$  according the finite differencing scheme described above, which we did over  $10^7$  time steps, again chosen to ensure statistical independence based on measurement of potential energy correlation. We then repeatedly sampled the potential energy every  $10^5$  time steps over a further  $10^7$  simulation time steps in order to estimate the probability of making ghost Monte-Carlo moves between different values of  $k$  and  $\phi$  as described in detail above. At each nearby value of  $(k, \phi)$  we obtained several independent estimates of the transition probabilities, and estimated the error from the standard deviation of the distribution of the independent estimates.

### 2. Pattern Registration in the Oscillating Pair Potential

We computed the radial distribution function  $g(r)$  for equilibrated snapshots of the oscillating pair potential system at  $k_B T = 0.25\epsilon$  and various values of  $k$  and  $\phi$  and compared it with the pair interaction potential  $U(r)$  in Fig. 10 to determine whether the decrease in free energy we found in the alchemical potential calculation (Fig. 4a, main text) could be detected in the pattern registration. Fig. 10 shows no clearly discernible difference in the pattern registration. Furthermore, in Fig. 11 we plot potential energy difference as a function of  $r$  at fixed  $k = 8.0$  between  $\phi = 0.55$  and  $\phi = 0.52$ , and see that over the range of the oscillating pair potential, the differences are less than 3% of  $\epsilon$ .

[1] D. Mendelejeff, *Berichte der deutschen chemischen Gesellschaft* **4**, 348 (1871).

[2] Mendeleeff, *J. Chem. Soc., Trans.* **55**, 634 (1889).

- [3] G. N. Lewis, *J. Am. Chem. Soc.* **38**, 762 (1916).
- [4] E. J. Holmyard, *Makers of Chemistry* (Oxford, Oxford, 1931).
- [5] C. Perrier and E. Segré, *J. Chem. Phys.* **5**, 712 (1937).
- [6] C. Perrier and E. Segré, *Nature* **159**, 24 (1947).
- [7] Z. Zhang and S. C. Glotzer, *Nano Lett.* **4**, 1407 (2004).
- [8] S. C. Glotzer and M. J. Solomon, *Nat. Mater.* **6**, 557 (2007).
- [9] A. B. Pawar and I. Kretschmar, *Macromol. Rapid Commun.* **31**, 150 (2010).
- [10] S. Sacanna and D. J. Pine, *Curr. Opin. Colloid Interface Sci.* **16**, 96 (2011).
- [11] G. Zhang, D. Wang, and H. Möhwald, *Angew. Chem., Int. Ed.* **44**, 7767 (2005).
- [12] D. J. Kraft, J. Groenewold, and W. K. Kegel, *Soft Matter* **5**, 3823 (2009).
- [13] Y. Wang, Y. Wang, D. R. Breed, V. N. Manoharan, L. Feng, A. D. Hollingsworth, M. Weck, and D. J. Pine, *Nature* **491**, 51 (2012).
- [14] G. van Anders, N. K. Ahmed, R. Smith, M. Engel, and S. C. Glotzer, *ACS Nano* **8**, 931 (2014), arXiv:1304.7545 [cond-mat.soft].
- [15] F. Lu, K. G. Yager, Y. Zhang, H. Xin, and O. Gang, *Nat. Commun.* **6**, 6912 (2015).
- [16] G. van Anders, D. Klotsa, N. K. Ahmed, M. Engel, and S. C. Glotzer, *Proc. Natl. Acad. Sci. U.S.A.* **111**, E4812 (2014), arXiv:1309.1187 [cond-mat.soft].
- [17] P. W. Anderson, *Science* **177**, 393 (1972).
- [18] K. H. Sandhage, *JOM* **62**, 32 (2010).
- [19] D. M. Teter, *MRS Bulletin* **23**, 22 (1998).
- [20] H. Paliwal and M. R. Shirts, *Journal of Chemical Theory and Computation* **7**, 4115 (2011).
- [21] V. M. O. Batista and M. A. Miller, *Phys. Rev. Lett.* **105**, 088305 (2010).
- [22] M. Dzugutov, *Phys. Rev. A* **46**, R2984 (1992).
- [23] M. Dijkstra and R. van Roij, *Phys. Rev. E* **56**, 5594 (1997).
- [24] M. Engel and H.-R. Trebin, *Phys. Rev. Lett.* **98**, 225505 (2007).
- [25] C. L. Phillips and G. A. Voth, *Soft Matter* **9**, 8552 (2013).
- [26] S. Sacanna, W. T. M. Irvine, P. M. Chaikin, and D. Pine, *Nature* **464**, 575 (2010).
- [27] M. Marechal, R. J. Kortschot, A. F. Demirörs, A. Imhof, and M. Dijkstra, *Nano Lett.* **10**, 1907 (2010), arXiv:1112.1209 [cond-mat.soft].
- [28] M. Marechal and M. Dijkstra, *Phys. Rev. E* **82**, 031405 (2010), arXiv:1007.0197 [cond-mat.soft].
- [29] J. de Graaf, R. van Roij, and M. Dijkstra, *Phys. Rev. Lett.* **107**, 155501 (2011), arXiv:1107.0603 [cond-mat.soft].
- [30] L. Rossi, S. Sacanna, W. T. M. Irvine, P. M. Chaikin, D. J. Pine, and A. P. Philipse, *Soft Matter* **7**, 4139 (2011).
- [31] Y. Zhang, F. Lu, D. van der Lelie, and O. Gang, *Phys. Rev. Lett.* **107**, 135701 (2011).
- [32] D. J. Kraft, R. Ni, F. Smalenburg, M. Hermes, K. Yoon, D. A. Weitz, A. van Blaaderen, J. Groenewold, M. Dijkstra, and W. K. Kegel, *Proc. Natl. Acad. Sci. U.S.A.* **109**, 10787 (2012).
- [33] P. F. Damasceno, M. Engel, and S. C. Glotzer, *ACS Nano* **6**, 609 (2012), arXiv:1109.1323 [cond-mat.soft].
- [34] R. Ni, A. P. Gantapara, J. de Graaf, R. van Roij, and M. Dijkstra, *Soft Matter* **8**, 8826 (2012), arXiv:1111.4357 [cond-mat.soft].
- [35] P. F. Damasceno, M. Engel, and S. C. Glotzer, *Science* **337**, 453 (2012), arXiv:1202.2177 [cond-mat.soft].
- [36] S. Sacanna, M. Korpics, K. Rodriguez, L. Colon-Melendez, S.-H. Kim, D. J. Pine, and G.-R. Yi, *Nat. Commun.* **4**, 1688 (2013).
- [37] A. P. Gantapara, J. de Graaf, R. van Roij, and M. Dijkstra, *Phys. Rev. Lett.* **111**, 015501 (2013).
- [38] A. Jain, J. R. Errington, and T. M. Truskett, *Soft Matter* **9**, 3866 (2013).
- [39] Y. Wang, Y. Wang, X. Zheng, G.-R. Yi, S. Sacanna, D. J. Pine, and M. Weck, *J. Am. Chem. Soc.* **136**, 6866 (2014).
- [40] S.-H. Kim, A. D. Hollingsworth, S. Sacanna, S.-J. Chang, G. Lee, D. J. Pine, and G.-R. Yi, *J. Am. Chem. Soc.* **134**, 16115 (2012).
- [41] J. A. Millan, D. Ortiz, and S. C. Glotzer, *Soft Matter* **11**, 1386 (2015).
- [42] M. Engel, P. F. Damasceno, C. L. Phillips, and S. C. Glotzer, *Nat. Mater.* **14**, 109 (2015).
- [43] N. K. Ahmed, G. van Anders, E. R. Chen, and S. C. Glotzer, Submitted (2015), arXiv:1501.03130 [cond-mat.mtrl-sci].
- [44] H. E. Haber and H. A. Weldon, *Phys. Rev. D* **25**, 502 (1982).
- [45] D. Yamada and L. G. Yaffe, *JHEP* **0609**, 027 (2006), arXiv:hep-th/0602074 [hep-th].
- [46] C. Shannon, *Bell System Technical Journal* **27**, 379 (1948).
- [47] E. T. Jaynes, *Phys. Rev.* **106**, 620 (1957).
- [48] C. H. Bennett, *J. Comp. Phys.* **22**, 245 (1976).
- [49] L. D. Landau and E. M. Lifshitz, *Statistical Physics, Part 1*, 3rd ed. (Butterworth-Heinemann, Oxford, 1980).
- [50] L. D. Landau and E. M. Lifshitz, *Theory of Elasticity*, 3rd ed. (Butterworth-Heinemann, Oxford, 1986).
- [51] R. D. Kamien, in *Soft Matter, Volume 3, Colloidal Order: Entropic and Surface Forces*, edited by G. Gompper and M. Schick (Wiley-VCH, Weinheim, 2007) Chap. 1, pp. 1–40.
- [52] F. A. Escobedo, *Soft Matter* **10**, 8388 (2014).
- [53] D. Frenkel, *Nat. Mater.* **14**, 9 (2015).
- [54] A. Haji-Akbari, M. Engel, A. S. Keys, X. Zheng, R. G. Petschek, P. Palffy-Muhoray, and S. C. Glotzer, *Nature* **462**, 773 (2009), arXiv:1012.5138 [cond-mat.soft].
- [55] E. Gilbert, D. Johnson, and S. Keerthi, *IEEE J. Robotics and Automation* **4**, 193 (1988).
- [56] E. R. Chen, D. Klotsa, M. Engel, P. F. Damasceno, and S. C. Glotzer, *Phys. Rev. X* **4**, 011024 (2014), arXiv:1309.2662 [cond-mat.soft].
- [57] J. A. Anderson and S. C. Glotzer, (2013), <http://codeblue.umich.edu/hoomd-blue>, arXiv:1308.5587 [physics.comp-ph].
- [58] Wöhler and Liebig, *Annalen der Pharmacie* **3**, 249 (1832).
- [59] B. Moulton and M. J. Zaworotko, *Chemical Reviews* **101**, 1629 (2001).
- [60] V. Venkatasubramanian, K. Chan, and J. Caruthers, *Computers & Chemical Engineering* **18**, 833 (1994).
- [61] M. Z. Miskin and H. M. Jaeger, *Nat. Mater.* **12**, 326 (2013).
- [62] B. Srinivasan, T. Vo, Y. Zhang, O. Gang, S. Kumar, and V. Venkatasubramanian, *Proc. Nat. Acad. Sci. U.S.A.* **110**, 18431 (2013).
- [63] M. Z. Miskin and H. M. Jaeger, *Soft Matter* **10**, 3708 (2014).
- [64] Y. Geng, P. F. Damasceno, and S. C. Glotzer, (2015).
- [65] M. Z. Miskin, J. J. de Pablo, and H. M. Jaeger, Preprint (2015).
- [66] F. Tonon, *Journal of Mathematics and Statistics* **1**, 8 (2004).
- [67] H. Georgi, *Lie Algebras in Particle Physics*, 2nd ed. (Westview Press, Boulder, Colorado, 1999).
- [68] B. Fornberg, *Mathematics of Computation* **51**, 699 (1988).
- [69] N. Metropolis, A. W. Rosenbluth, M. N. Rosenbluth, A. H. Teller, and E. Teller, *J. Chem. Phys.* **21**, 1087 (1953).
- [70] S. Y. Park, A. K. R. Lytton-Jean, B. Lee, S. Weigand, G. C. Schatz, and C. A. Mirkin, *Nature* **451**, 553 (2008).
- [71] M. R. Jones, R. J. Macfarlane, B. Lee, J. Zhang, K. L. Young, A. J. Senesi, and C. A. Mirkin, *Nat. Mater.* **9** (2010), 10.1038/nmat2870.
- [72] E. Auyeung, R. J. Macfarlane, C. H. J. Choi, J. I. Cutler, and C. A. Mirkin, *Advanced Materials* **24**, 5181 (2012).
- [73] Y. Kim, R. J. Macfarlane, and C. A. Mirkin, *J. Am. Chem. Soc.* **135**, 10342 (2013).

- [74] C. Zhang, R. J. Macfarlane, K. L. Young, C. H. J. Choi, L. Hao, E. Auyeung, G. Liu, X. Zhou, and C. A. Mirkin, *Nat. Mater.* **12**, 741 (2013).
- [75] K. L. Young, M. B. Ross, M. G. Blaber, M. Rycenga, M. R. Jones, C. Zhang, A. J. Senesi, B. Lee, G. C. Schatz, and C. A. Mirkin, *Advanced Materials* **26**, 653 (2014).
- [76] R. Macfarlane, M. Jones, A. Senesi, K. Young, B. Lee, J. Wu, and C. Mirkin, *Angew. Chem., Int. Ed.* **49**, 4589 (2010).
- [77] M. R. Jones, R. J. Macfarlane, B. Lee, J. Zhang, K. L. Young, A. J. Senesi, and C. A. Mirkin, *Nat. Mater.* **9**, 913 (2010).
- [78] R. J. Macfarlane, B. Lee, M. R. Jones, N. Harris, G. C. Schatz, and C. A. Mirkin, *Science* **334**, 204 (2011).
- [79] M. M. Maye, M. T. Kumara, D. Nykypanchuk, W. B. Sherman, and O. Gang, *Nat. Nano.* **5**, 116 (2010).
- [80] Y. Zhang, F. Lu, K. G. Yager, D. van der Lelie, and O. Gang, *Nat. Nano.* **8**, 865 (2013).